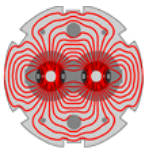

LHC Project Note 395

2007-01-22

Christine.Hoa@cern.ch

Procedures and first investigation of the power radiated by proton-proton collisions into an early separation dipole for the LHC Luminosity Upgrade

Christine Hoa / AT-MCS

Keywords: insertion region, proton-proton collisions, radiated energy, luminosity upgrade

Summary

In this note, a simplified model of a proton-proton collisions and a dipole is used to investigate the variation of the impinging energy versus the distance to the interaction point (IP) and the dipole inner coil diameters. Contrary to expectation, the impinging energy is not seen to vary significantly with the distance to the IP and even tends to decrease when the distance is decreased. On the contrary, the inner coil diameter is a sensitive parameter.

In order to understand these observations and allow predictions, the losses and their variations are analysed in terms of secondary particle types and energy spectrum. For any designed optical set up, it gives some hints on the critically 'hot' regions.

1. Introduction

The early separation scheme [3] requires a small dipole positioned deeply inside the LHC experimental detectors. Likewise, a significant luminosity upgrade benefits from a reduced distance between the IP and the triplets [3]. Given the much increased luminosity and the reduced distance to the IP, a critical issue, in both cases, is the potential large increase of the energy and dose received by the magnets. As a first step in the investigations, we study here the energy impinging on a very simplified model of dipole as a function of its position and aperture. The collision as well is simplified, assuming a point like co-linear collision. It is believed that this simplified model still retains the essentials of the physics involved. The impinging energy is studied in terms of the family and spectra of impinging particles to shed some light on the non-intuitive results.

2. Proton-proton collisions at center of mass of 14 TeV

2.1 Luminosity, Cross-section and Total power

The goal of the luminosity upgrade is to increase by a factor 10 the nominal LHC luminosity to reach $L=10^{35}$ $cm^{-2}s^{-1}$. The total cross section is assumed to be A=80 mbarn, where:

- 20 mbarn are single diffractive events: one of the primary protons maintains its own identity while the other one transforms into reaction products.

This is an internal CERN publication and does not necessarily reflect the views of the LHC project management.

- 60 mbarn are inelastic non diffractive events: Both primary protons transform in a cascade of secondary particles.

The elastic scattering (40 mbarn) has been neglected as the scattered protons do not interact with the insertion region elements but, after several revolutions, they would be absorbed by the collimator systems.

According to the formulation (1), in terms of total power, the radiated energy will represent 18 kW from the p-p collisions at center of mass of 14 TeV, assuming the total cross section of 80 mbarn.

$$Power(W) = Power(eV/primary) * e(eV) * L(cm^{-2}s^{-1}) * A(barn) * 10^{-24} \quad (1)$$

$$18 * 10^{3} = 14 * 10^{12} * 1.609 * 10^{-19} * 10^{35} * 80 * 10^{-3} * 10^{-24}$$

2.2 Secondary Particles and decay

In the insertion region, after the p-p collisions, the debris consist mostly of protons, electrons and positrons, photons, neutrons, charged and neutral pions or pionzeros (Figures 1 and 2). The multiplicity is around 120 secondary particles generated per collision. It has to be noted that the charged and neutral pions represent a great part of the secondary particles in terms of mean number but, also in terms of energy. The spectra will be analysed in the following sections.

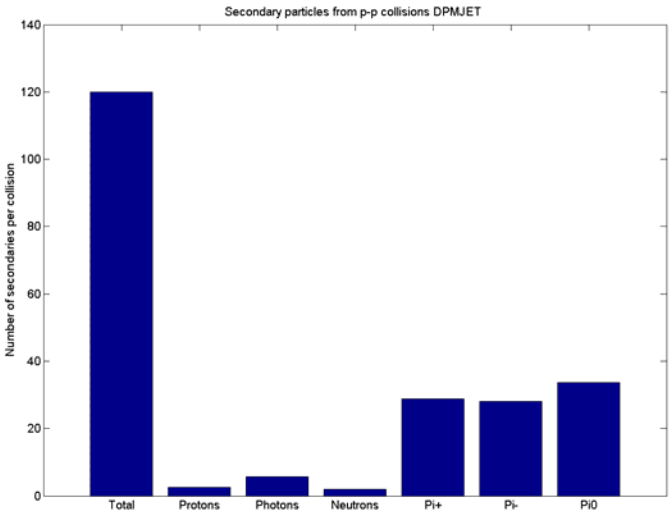

Figure 1: histogram of the mean number of secondary particles/ p-p collision

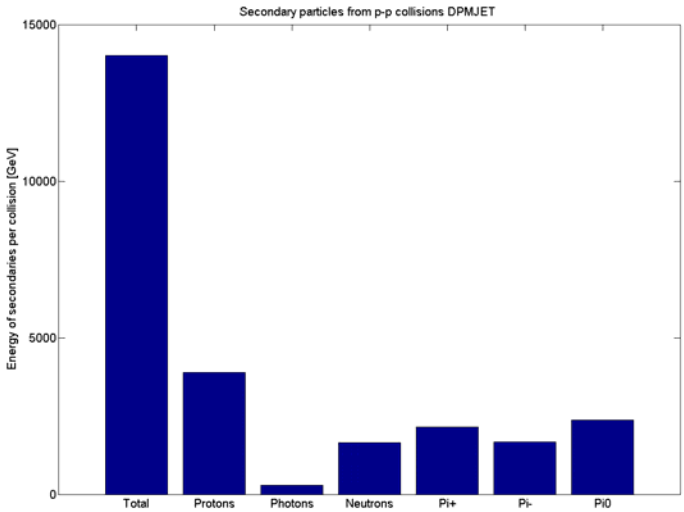

Figure 2: histogram of energy of secondary particles/ p-p collision

The mean life time τ and the decay of secondary particles are described in Table I. The secondary particles are mostly stable and will flow without decaying in the insertion region. With an exponential decaying law, at the mean life time, about 63% of the particles have decayed. The distributions of the mean distances traveled by pions+, pion- and pionzeros in the laboratory frame are plotted in Figure 3, Figure 4, and Figure 5, taking into account the relativistic factors γ and β. The mean distance d is calculated with the following formula:

$$d = \beta * \gamma * c * \tau \quad (2)$$

The pionzeros decay just after the collision into 2 photons in 98.798% probability: the average mean distance over a statistics of 100 p-p collisions is $1.2*10^{-5}$ m. A great majority of

pions + and pions - are travelling through the whole insertion region. The average mean distances are respectively $4.0*10^3$ m and $3.4*10^3$ m.

Secondary particles	**τ Mean life time**	**Decay products**
Protons	Stable $> 10^{30}$ years	-
Electrons and positrons	Stable	-
Photons	Stable	-
Neutrons	Unstable 885.7 s	$n \rightarrow p + e^- + \bar{\nu}_e$
Pions + Pions -	$2.6*10^{-8}$ s	$\pi^+ \rightarrow \mu^+ + \nu_\mu, \pi^- \rightarrow \mu^- + \bar{\nu}_\mu (99.9877\%)$ $\pi^+ \rightarrow e^+ + \nu_e, \pi^- \rightarrow e^- + \bar{\nu}_e (0.0123\%)$
Pionzeros	$0.84*10^{-16}$ s	$\pi^0 \rightarrow 2\gamma (98.798\%)$ $\pi^0 \rightarrow \gamma + e^+ + e^- (1.198\%)$

Table I: Mean life time and decay of secondary particles

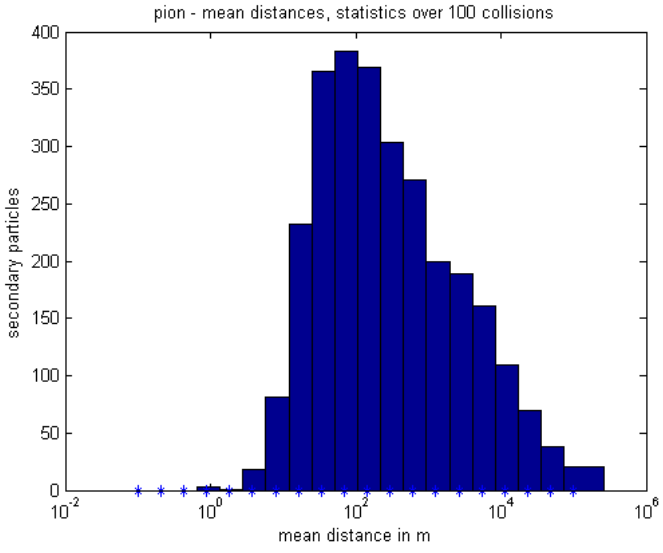

Figure 3: Distribution of mean distances for pions -

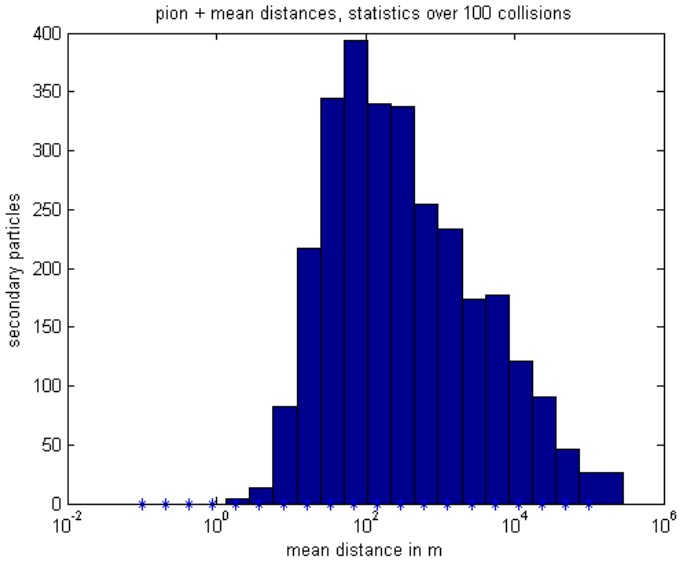

Figure 4: Distribution of mean distances for pions +

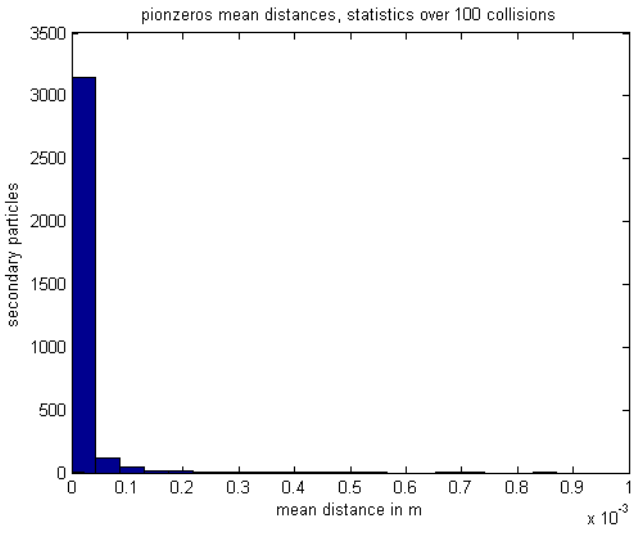

Figure 5: Distribution of mean distances for pionzeros

3. Source generator and Multi-particle tracking

The DPMJET III event generator has been used to generate the proton-proton collisions at 14 TeV in centre of mass. In fact, in this range of energy for protons, it is PYTHIA v6.11 event generator that is called by DPMJET III. A detailed analysis can be found in [4] when different event generators for the p-p collisions at high energy have been assessed. In this note, the events are assumed head on, point like bunches collisions at the interaction point (IP). There is no Xing angle specified for the two proton beams.

For the particle tracking and energy transport, the Monte Carlo code FLUKA [5], [6] has been used. FLUKA tracks the secondary particles from the interaction point to the vacuum chamber in the experiment region and up to 33 meters after the IP. The study consists in evaluating the energy flow at different longitudinal location along the axis for a given Insertion Region element such as a Copper dipole. The energy flow results from FLUKA are expressed in GeV/primary, and are transformed into Watts with the formulation (1), taking into account the interaction rate of the p-p collisions in a high luminosity environment (A=80 mbarn, $L=10^{35}$ $cm^{-2}s^{-1}$).

For the tracking and energy transport, the cut off parameters are specified by default by FLUKA and given in Table II. The FLUKA outputs show that the energy radiated below the specified thresholds is totally negligible, so it means the complete interaction cascades are tracked. An optimisation of the energy cut off parameters is not needed: energy deposition in material region is not requested as energy is stocked in Blackhole: therefore CPU time is short and varies from 2 to 20 minutes depending on the location from the IP.

For neutron energy transport, there is a distinction for high and low energy neutrons: for energy below 19.6 MeV, a multigroup algorithm is performed by FLUKA where elastic and inelastic reactions are simulated by group to group transfer probabilities.

Number of primary particles	5 runs of 2000
CPU time/ run	Around 2 to 20 minutes
Cut off energy for photons	< 3 keV in the dipole and beam pipe
Cut off energy for e-/+e-	<30 keV in the dipole and beam pipe
Cut off energy for Muons	<100 keV
Cut off energy for Hadrons	<100 keV
Cut off for high energy neutrons	< 19.6 MeV
Cut off for low energy neutrons	<1E-14 GeV 72 neutron energy groups down to thermal energies

Table II: FLUKA computing parameters

4. Characterization of the secondary particles

The spatial distribution of particles is generally expressed in hadron physics in terms of the pseudo-rapidity η rather than the physical angle θ (angle of the particle trajectory relative to the beam axis).

$$\eta = -\ln(\tan(\frac{\theta}{2})) \tag{3}$$

To give some representative values, if we consider the position of Q1, the first insertion quadrupole magnet located at 23 m from the IP, the corresponding pseudo-rapidity is in the ranger of [6.8;7.4]. The corresponding θ angle relative to the beam axis is in the range of $[10^{-3}$; $2.10^{-3}]$ in radians. The spatial distribution of the secondary particles (Figure 6) is symmetric with respect to the transverse axis (η=0, θ=π/2). The particles have a peak distribution around η=-4 and η=4, in the transverse direction. The number of secondary particles decreases with increasing pseudo rapidity or decreasing θ angle relative to the beam axis. Figure 7 brings information on the energy distribution of the secondary particles in the space. If the number of secondaries is larger near the transverse direction, most of the energy is distributed symmetrically in the very forward direction of the beam. The 2 peaks are observed for a pseudo rapidity of -8 and 8, which correspond to very small polar angles ($<10^{-3}$ rad). They could be interpreted as only one peak with an integration step for θ of 1 mrad. In fact N is also small, so the precision is less in this range of small polar angle and a larger integration step is justified. The peak shows the energetic particles in the very forward direction of the beam.

At the triplet location where η≈7, it can be observed that both the number of particles received and their total energy varies rapidly with small changes of geometry or transverse and longitudinal positions.

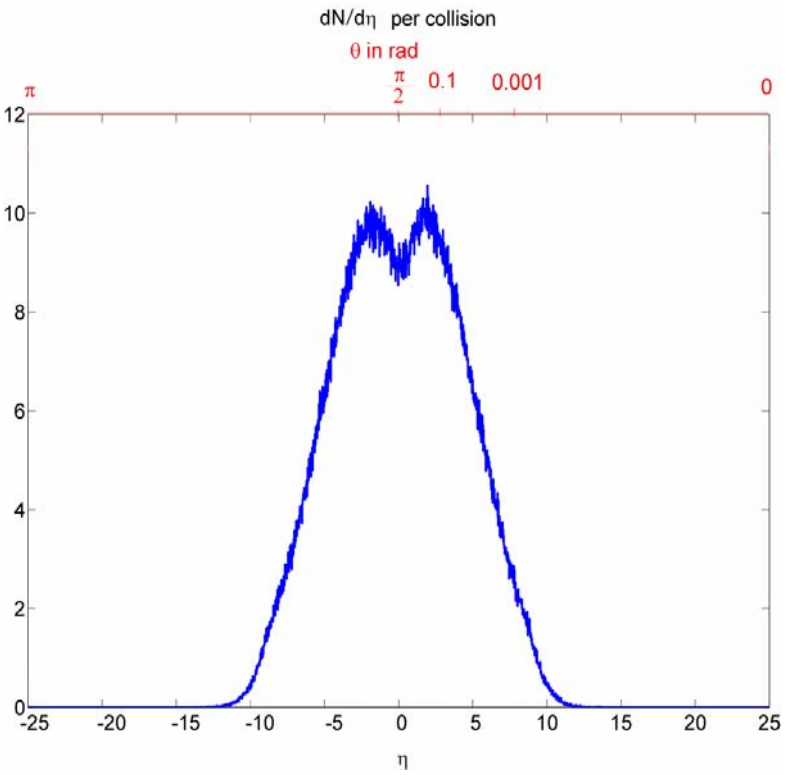

Figure 6: Variation of number of secondary particle with pseudo-rapidity

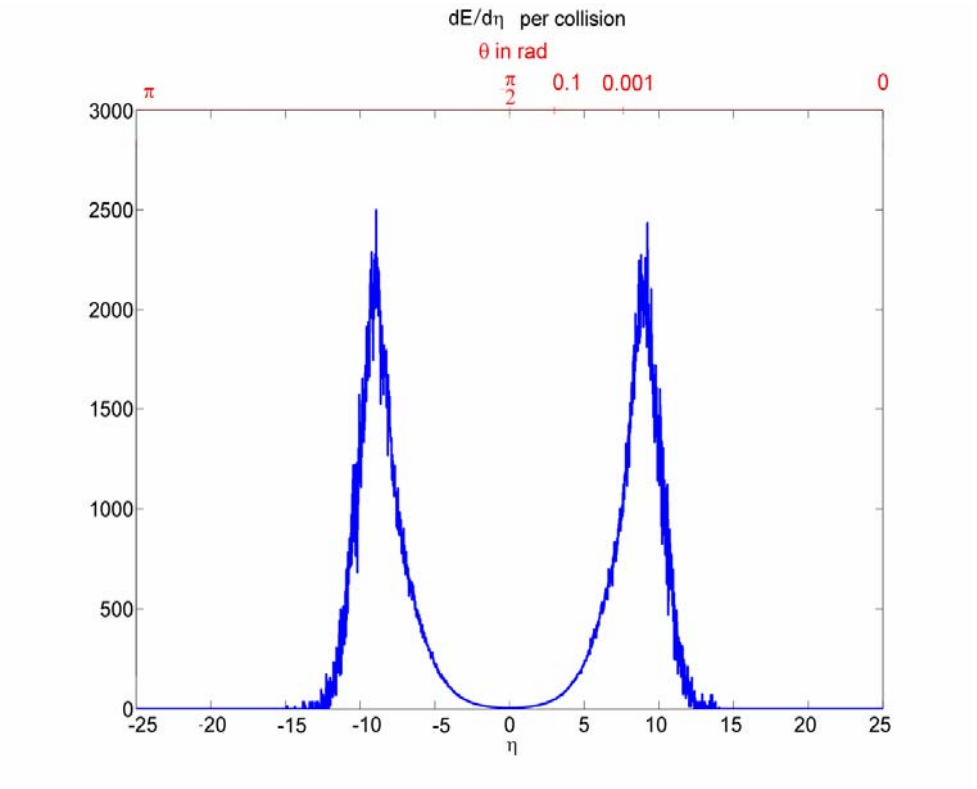

Figure 7: Variation of secondary particle energy with pseudo-rapidity

5. Impinging power on a short magnet

For this calculation, we concentrate on the coil of a small dipole with dimensions suitable for an early separation scheme.

5.1 Magnet model and layout

The dipole is represented by its superconducting coil modelled as a simple hollow cylinder. For later studies, the dominant material, copper, is assumed. The cylinder is surrounded by several total absorbers in order to evaluate the repartition of the power impinging the dipole on its front and inner faces and the power escaping through its gap to the beam pipe. The dipole front face is located at 3.5 m from the collisions point (Figure 8), in a position that appears space-wise possible in the ATLAS experiment. A surrounding black hole in a form of a box is used to collect all particles that are neither flowing inside the solid angle defined by the dipole outer surfaces nor escaping through the beam pipe vacuum chamber.

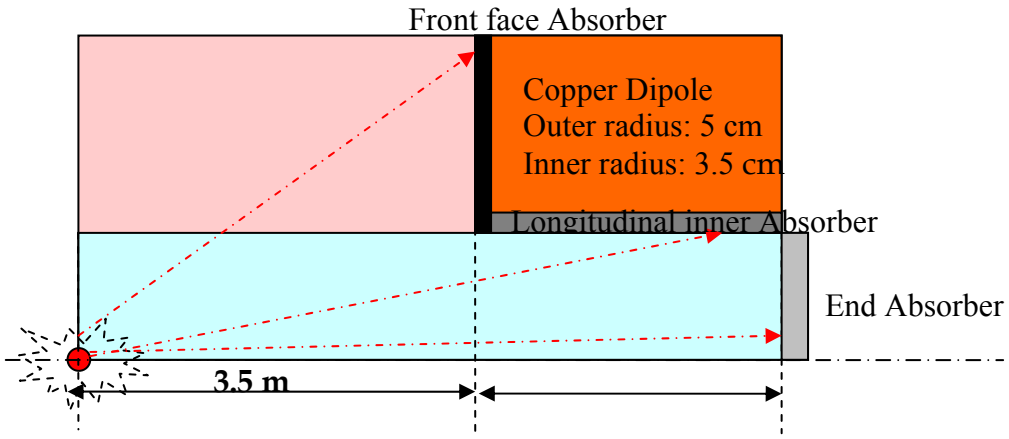

Figure 8: FLUKA model with total absorbers for detailed power distribution

5.2 Impinging Power at z=350 cm

5.2.1 Front surface and longitudinal inner surface

Table III gives the repartition of the power in the model. The power impinging the dipole material is 209W, i.e. only about 1% of the total power radiated by the hadron collisions. Within the solid angle defined by the dipole, most of the power escapes through the gap as the energetic particles are flying in the very forward direction (Figure 8). The contributions of the power impinging the dipole through the front surface and the longitudinal inner surface are almost equally balanced.

Adding this power to that collected by the black hole, we recover the 18 kW of the total power due to the collision of 2 proton beams of 7 TeV, demonstrating the consistency of the simulation by FLUKA.

Details Power distribution	(W)
Power impinging the front surface	110.2
Power impinging the longitudinal inner surface	98.8
Power escaping through the magnet gap	8421.1
Power in the surrounding BlackHole	9378.4
Total	18008.5

Table III: Details in Power distribution

5.2.2 Charge and energy of impinging secondary particles

The debris of the proton-proton collisions impacting the dipole are composed of almost 2/3 of charged particles and 1/3 of neutrals (over all events, the electric charge is indeed conserved). The negative and the positive charged particles contributions in power have similar values (Table IV).

The power spectra of the debris travelling through the front face (Figure 9), or the longitudinal inner surface (Figure 10) are similar and show that the energy of the secondary particles hitting the magnet is 40 GeV on average, mostly distributed in the range of 20 to 100 GeV. The particles of higher energies flow through the magnet gap to the vacuum chamber (Figure 11). For the latter, the charge asymmetry due to the global charge conservation is very noticeable.

Power distribution for $L=L_0$	Front	Longitudinal	Magnet gap
Negative charged	33.5 W	27.7 W	1.19 kW
Positive charged	35.0 W	32.4 W	4.01 kW
Neutrals	41.7 W	38.6 W	3.22 kW
Total	110.2 W	98.8 W	8.42 kW

Table IV: Impinging power distribution due to charged and neutral particles

5.2.3 Power contribution per family of impinging particles

The contributions of the impinging power on the dipole region, per particle family are described in the Table V.

Particle family	Secondary particles	Front	Longitudinal	Magnet gap
Bosons	Photons	31.3 W	28.6 W	1.53 kW
Leptons	Electrons/positrons	4.3 W	5.1 W	11.2 W
	Muons	0.1 W	0.1 W	0.82 W
Hadrons	Protons	2.7 W	2.4 W	2.50 kW
	Neutrons	2.2 W	2.4 W	1.07 kW
	Pions + and pions -	50.5 W	43.7 W	2.23 kW

Table V: Power distribution per type of particle family

The major contributors of flowing energy in the dipole, both through the front surface and the longitudinal inner surface are pions and photons. The photons are original secondary photons and also result from the decay of pionzeros. The high energy protons (2.5 kW)) and neutrons (1.07 kW) are flowing in the very forward direction without impacting the dipole (see Figure 14).

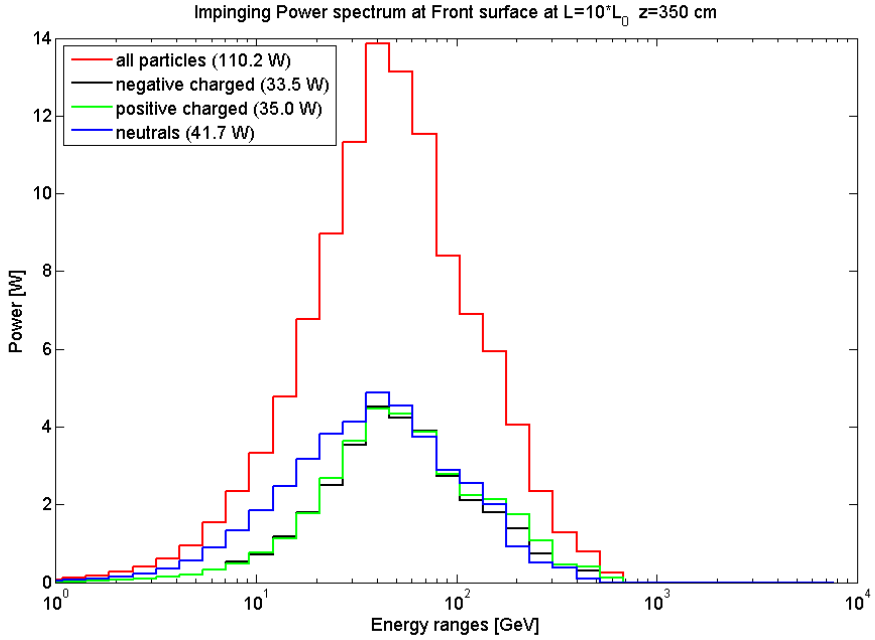

Figure 9: Impinging power spectrum at the front face, z=350 cm

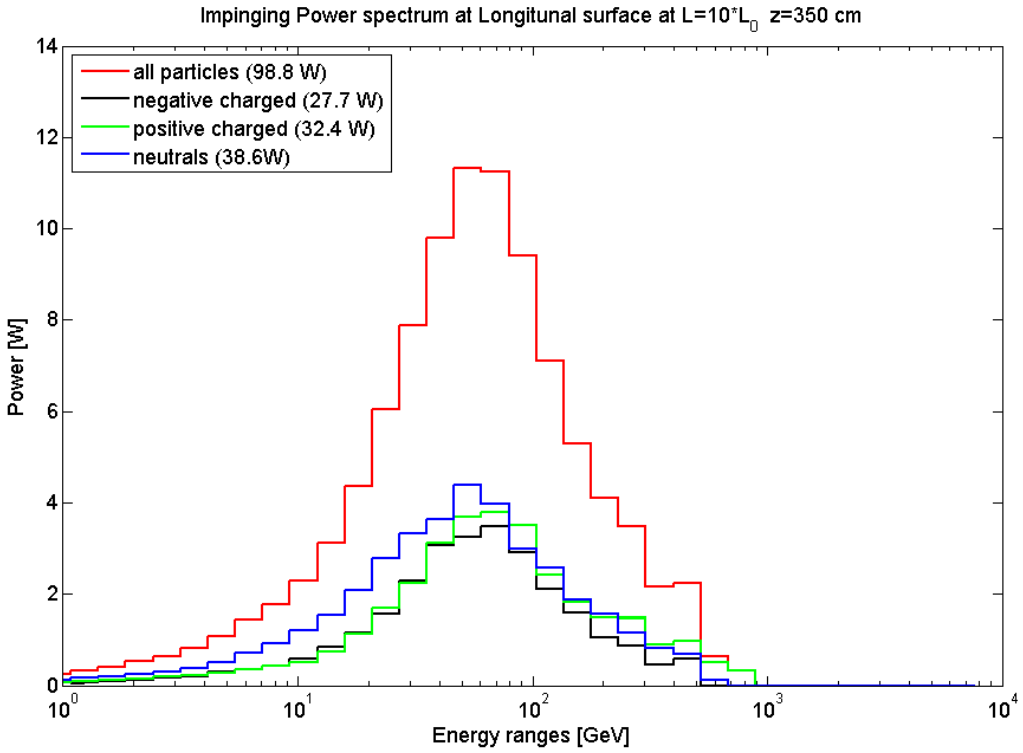

Figure 10: Impinging power spectrum at the longitudinal inner surface, z=350 cm

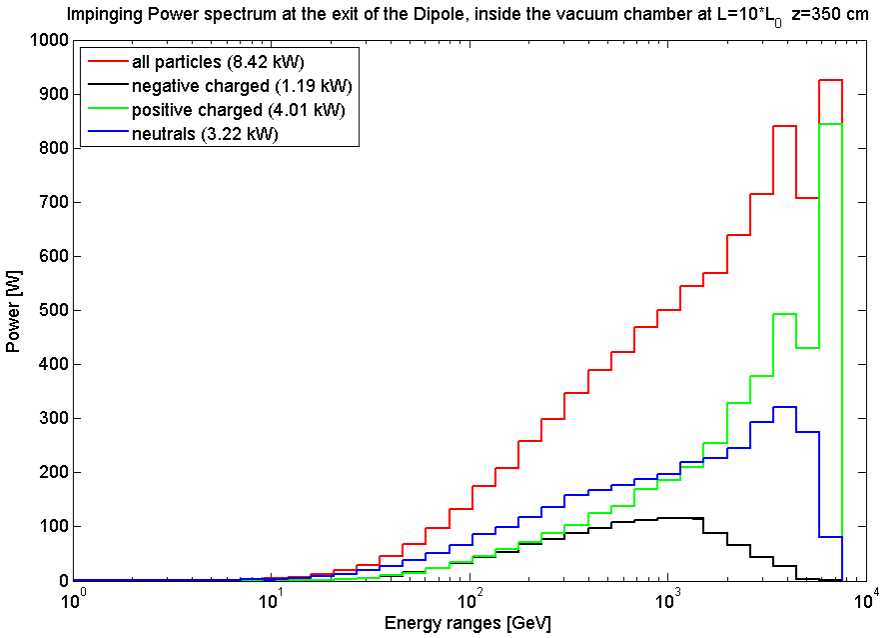

Figure 11: Power spectrum of particles travelling through the magnet gap, z=350 cm

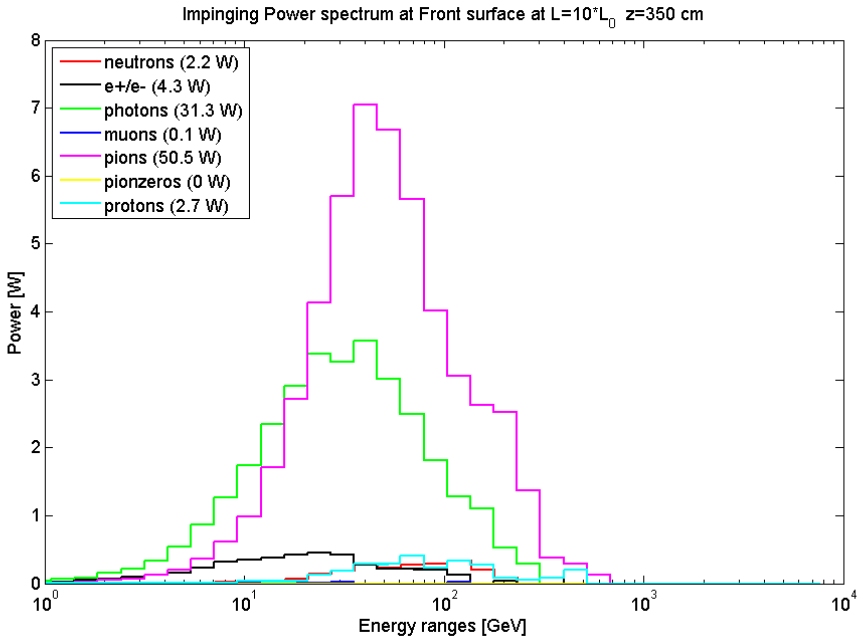

Figure 12: Particle families impinging the front face, z=350 cm

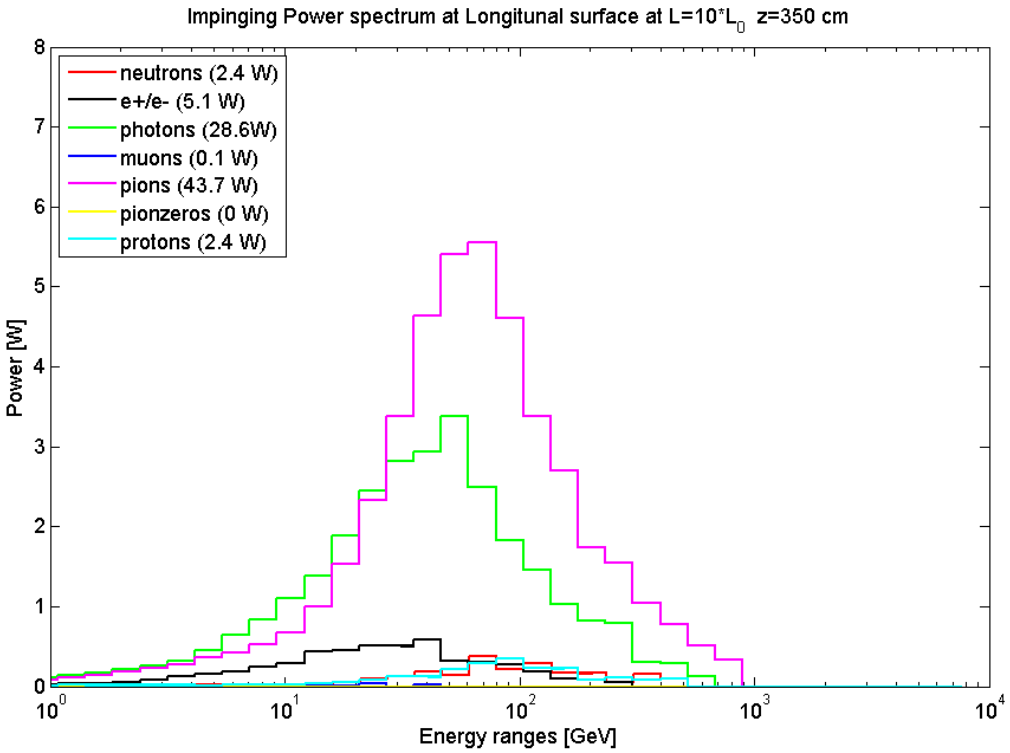

Figure 13: Particle families impinging the longitudinal inner surface, z=350 cm

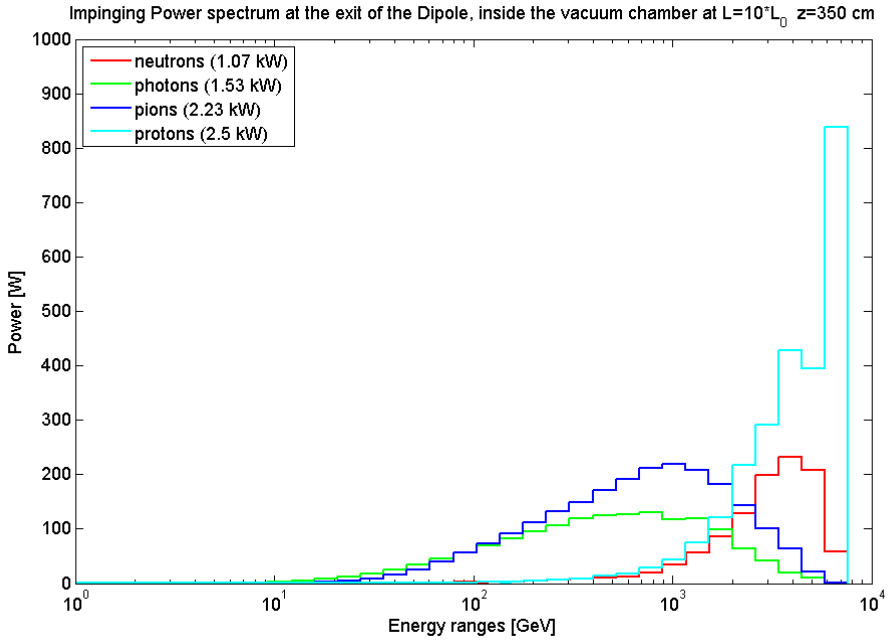

Figure 14: Particle families travelling through the magnet gap, z=350 cm

5.3 Variation of the impinging power with the dipole longitudinal position

5.3.1 Impinging power

All simulations were done so far for the preferred dipole position at 3.5 m from the IP. In this section, we investigate the variation of impinging power if the longitudinal position of the dipole varies.

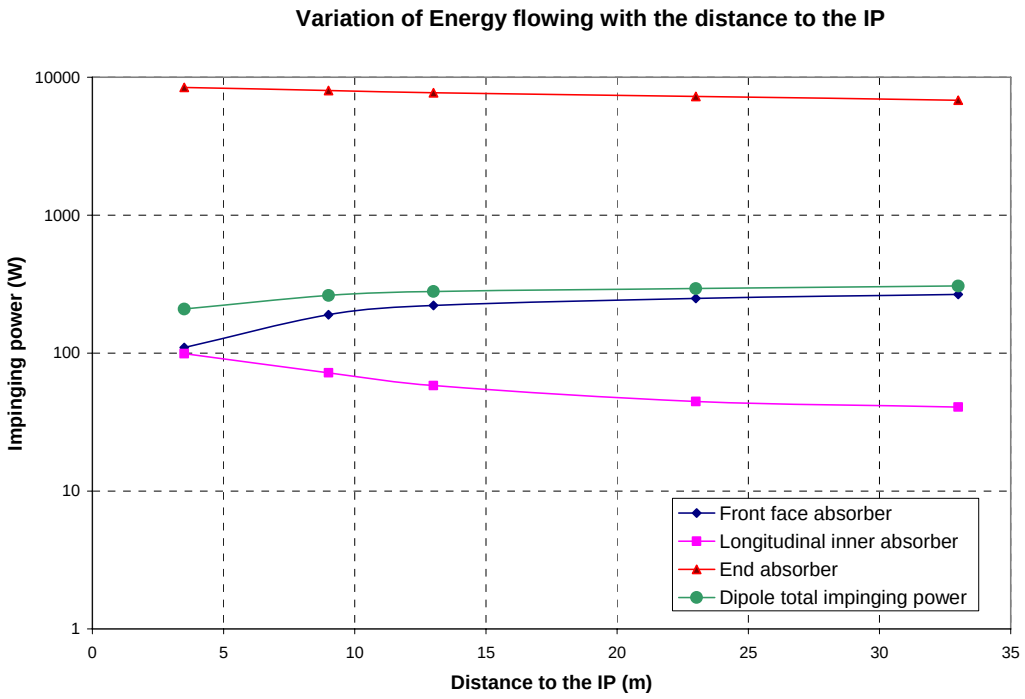

Figure 15: Variation of impinging power with the distance to the IP

For a fixed dipole geometry, the total impinging energy increases moderately with the distance to the interaction point, although the solid angle defined by the dipole decreases (Figure 15). This moderate variation hides two opposing processes with much larger variations: on one hand, the power impinging the inner dipole surface decreases significantly when the distance to the IP is increased; on the other hand, the power impinging on the front face increases significantly. Figure 16 illustrates these opposing variations of the impinging power.

This complex dependence on the angle is of relevance for shielding purposes. In order to shed some light, we investigate in the next section the variation of the power spectrum with the distance to the IP.

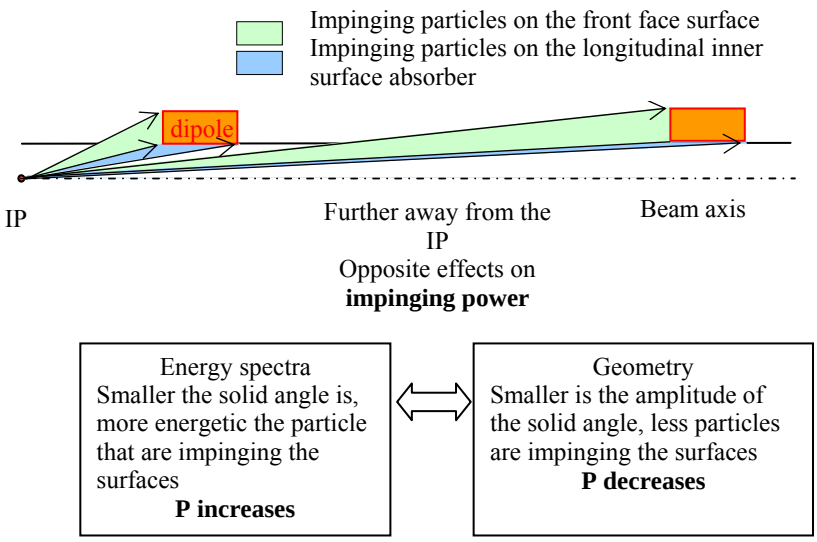

Figure 16: Schematic of the particles impinging the absorbers

5.3.2 Power spectrum evolution

For particles entering the front face and the longitudinal inner surface, the power spectra shifts towards the higher energy ranges when the dipole region is moved along the beam axis (see Figure 17, Figure 18). In the case of the front face, the peak values of the spectra increase and reach a maximum of 200 GeV at z=2300 cm. Then the peak starts to decrease at z=3300 for particles in the range of 300-400 GeV. On the contrary, for the longitudinal inner surface, the impinging particles have spectra that flatten when the dipole region is moved along the beam axis. The increase of particle energy is also less than observed for the front face.

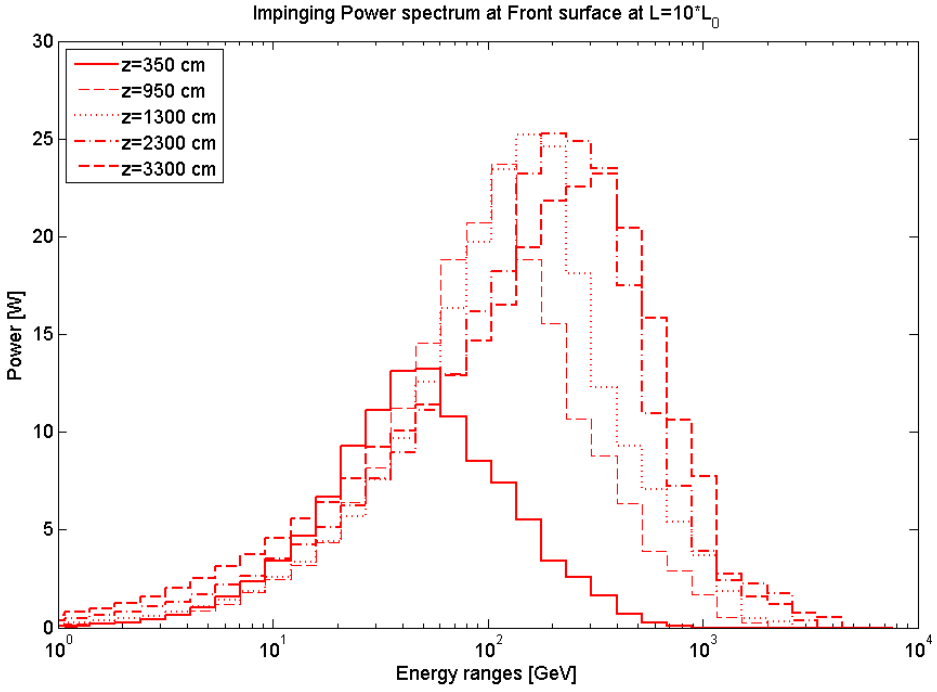

Figure 17: Evolution of the power spectrum at the Front face with the distance to the IP

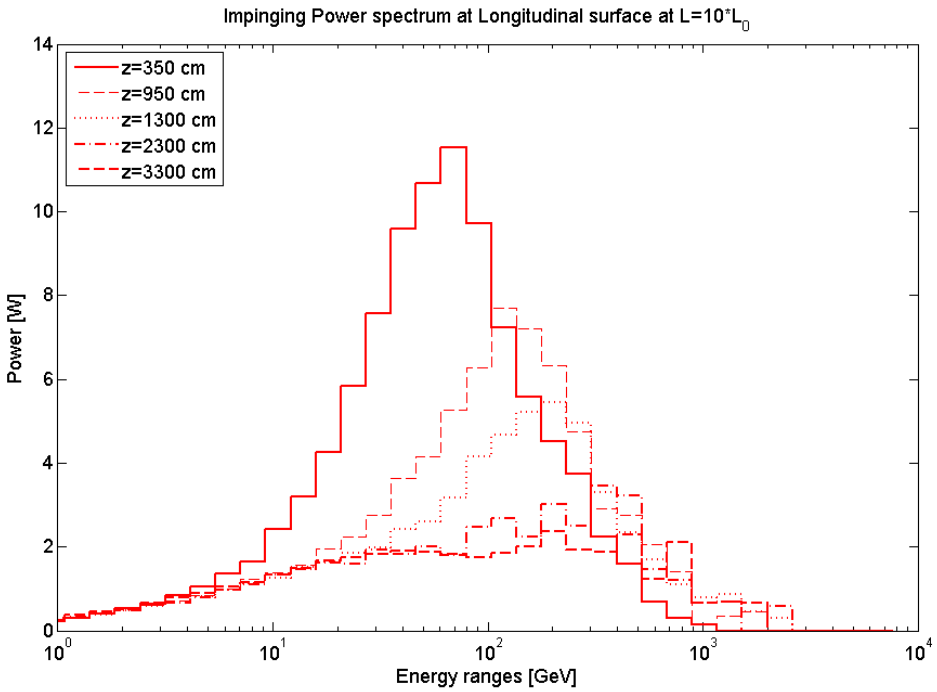

Figure 18: Evolution of the power spectrum at the longitudinal inner surface with the distance to the IP

5.4 Variation of the impinging Power with the dipole gap size

The FLUKA model described in Figure 8 was modified to investigate the influence of the magnet aperture diameter for a dipole at z=350 cm. The aperture diameter was increased from 70 mm to 110 mm. The 1.5 cm thickness for the dipole coil has been kept. The total impinging power on the dipole region (front face+ longitudinal inner surface) decreases from 209 W to 127 W. With an aperture of 110 mm, the secondary particles intercept the dipole region with a larger solid angle and therefore:

- The energy spectra are slightly shifted towards the lower energy ranges (Figure 19, Figure 20).
- The impinging powers on the front face and the longitudinal surface decrease by a factor of 2 for neutrons, e+/e-, photons and protons. The decrease is a bit less for pions (Table VI).

Secondary particles	Neutrons	e+/e-	Photons	Pions	Protons
Front face Aperture 70 /110 mm	2.2 /1.7 W	4.3/1.7 W	31.3/15.9 W	50.5/26.3 W	2.7/1.5 W
Longitudinal inner surface Aperture 70 /110 mm	2.4/1.2 W	5.1/2.1 W	28.6/19.4 W	43.7/32.0 W	2.4/1.8 W
Magnet gap Aperture 70/110 mm	1.07/1.08 kW	11.2/10.9 W	1.53/1.61 kW	2.23/2.31 kW	2.50/2.48 kW

Table VI: Evolution of the power distribution with the increase of the aperture dipole

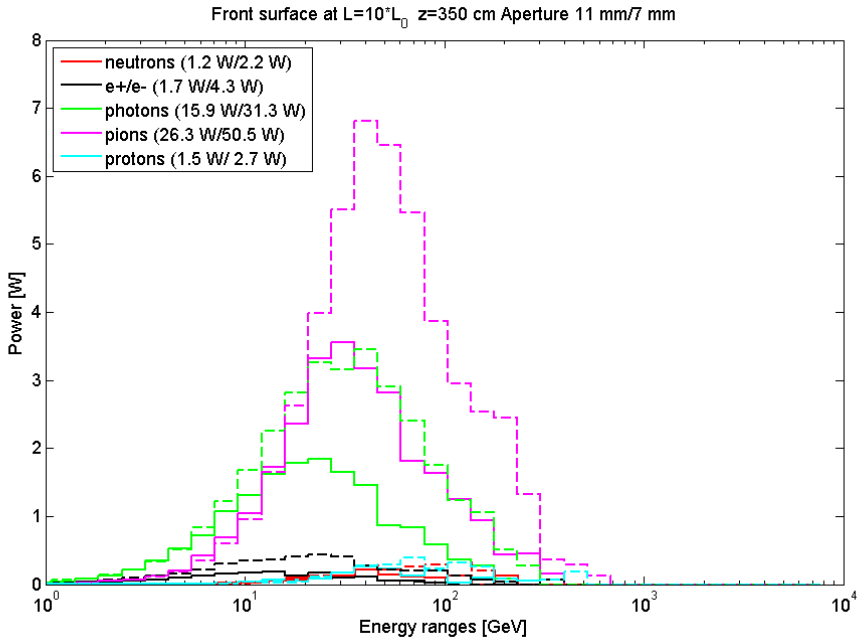

Figure 19: Front face, z=350 cm, L=L_0 , Aperture 110 mm (plain)/70 mm (dotted)

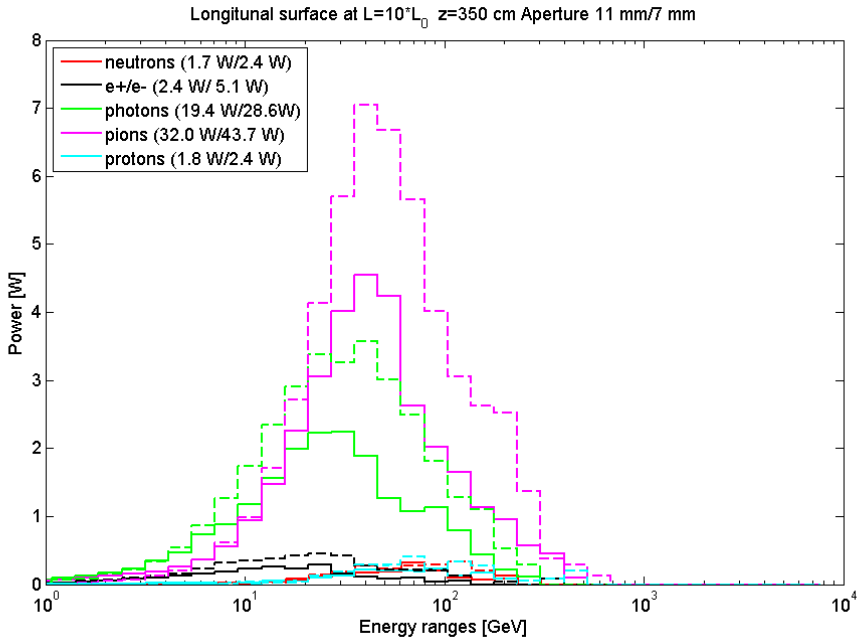

Figure 20: Longitudinal surface, z=350 cm, Aperture 110 mm (plain)/70 mm (dotted)

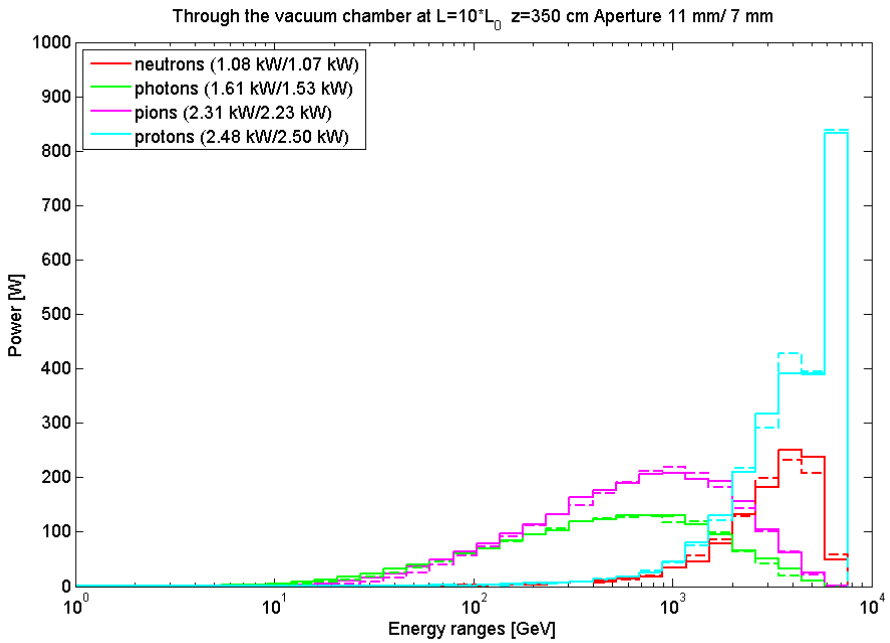

Figure 21: Through the vacuum chamber z=350 cm,

Aperture 110 mm (plain)/70 mm (dotted)

6. Conclusions

As a first step in the investigation of the power deposited into insertion elements, this study deals exclusively with the power impinging on them. Only a fraction of this energy will be absorbed. The study is carried out for the conditions of the luminosity upgrade, namely a center of mass energy of 14 TeV and a luminosity of $L=10^{35}$ $cm^{-2}s^{-1}$ .The total power received is complemented by the energy spectra and the distribution in particle families to have some understanding on the main contributors of impinging power on the insertion elements, such as a small dipole.

At z=350 cm, the impinging power for a pseudo-rapidity of 5.3 (dipole of aperture 70 mm and 15 mm coil thickness) is around 209 Watts. Photons and pions are by far the main contributors, impacting the dipole region equally through the front face and the longitudinal inner surface.

Most of the very energetic particle debris travels in the very forward direction through the magnet gap. The parametric study shows that:

- The impinging power increases moderately when the dipole moves farther away from the interaction point. This unexpected result stems from compensation between two significantly varying processes (loss on the front face or inner surface) and should be relevant for shielding or choice of materials. In other words, the energy received by a dipole at 3.5m is slightly less than the energy it would receive at 23m, i.e. the incident energy is not a show-stopper.

- The impinging power decreases significantly when the aperture of the dipole is increased. A reduction by a factor of about 2 can be gained with an increase of aperture from 70 mm to 110 mm.

This study shall be complemented by the evaluation of the power actually deposited in the magnet material.

The proton-proton collisions have been assumed to be head on, point like bunch collisions and no magnetic field have been taken into account. Further investigations shall be performed to estimate the effects of both a crossing angle of the colliding beams and the magnetic field of the dipole and also the one from the solenoid of the experiment.

7. Acknowledgments

I would like to thank Alfredo Ferrari, Francesco Cerutti, Markus Brugger and Stephan Roesler for their great help and support with the FLUKA modelling.

I am also very thankful to Jean Pierre Koutchouk, Elena Wildner, Guido Sterbini (AT/MCS/MA) for their stimulating discussions concerning the interpretation of the data. I would like also to acknowledge Francesco Broggi from INFN: our fruitful collaboration has brought some precious indications and advices for energy deposition studies in the triplet region.

References

[1] 'Particle Losses in the LHC Interaction Regions', K. Eggert and A. Morsch, CERN AT/93-17, LHC Note 229, June 1993.

[2] 'Local Power distribution from Particle losses in the LHC Inner Triplet Magnet Q1', A. Morsch, CERN AT/94-06, LHC Note 265.

[3] 'Investigations of the parameter space for the LHC Luminosity Upgrade', J-P Koutchouk, EPAC, June 2006.

[4] 'Comparison of the Monte-Carlo models for proton-proton interactions DPMjet and DTUjet' G. Sterbini, December 2006.

FLUKA licence references:

[5] 'FLUKA: a multi-particle transport code', A. Fasso`, A. Ferrari, J. Ranft, and P.R. Sala, CERN-2005-10 (2005), INFN/TC_05/11, SLAC-R-773

[6] 'The physics models of FLUKA: status and recent developments', A. Fasso`, A. Ferrari, S. Roesler, P.R. Sala, G. Battistoni, F. Cerutti, E. Gadioli, M.V. Garzelli, F. Ballarini, A. Ottolenghi, A. Empl and J. Ranft, Computing in High Energy and Nuclear Physics 2003 Conference (CHEP2003), La Jolla, CA, USA, March 24-28, 2003, (paper MOMT005), eConf C0303241 (2003), arXiv:hep-ph/0306267.